Proceedings of the ASME 2013 Conference on Smart Materials, Adaptive Structures and Intelligent Systems
SMASIS2013
September 16-18, 2013, Snowbird, Utah, USA

SMASIS2013-3204

DIMENSIONALLY STABLE OPTICAL METERING STRUCTURES WITH NITI COMPOSITES FABRICATED THROUGH ULTRASONIC ADDITIVE MANUFACTURING

Phillip Evans
MIT Lincoln Laboratory
Lexington, MA, USA

Marcelo Dapino
Ohio State University
Columbus, OH, USA

Ryan Hahnlen
Honda R&D Americas, Inc.
Raymond, OH, USA

Joshua Pritchard
Ohio State University
Columbus, OH, USA

ABSTRACT

High performance optical metering structures in airborne and space applications need to exhibit dimensional stability in demanding thermal and mechanical environments. Materials for this application should have a low coefficient of thermal expansion, high thermal diffusivity, high specific stiffness and exhibit good ductility. Current materials are limited in one or more of these properties. Common choices are invar, carbon-fiber composite, and silicon-carbide. The former has low specific stiffness and thermal diffusivity and the latter choices are brittle materials that require special care and have slow manufacturing processes. In this work, the development of a thermally invariant metal matrix composite will be described along with its incorporation into a high performance optical metering structure. The material is a composite of super-elastic NiTi ribbons and aluminum, where the ribbons are embedded using ultrasonic additive manufacturing. Measurements and modeling of the thermo-elastic response will be presented followed by the design and manufacture of a metering structure. The metering structure design eases integration with an optical bench and lens bezels while leveraging the advantageous properties of this new metal matrix composite.

INTRODUCTION

The development of a metal matrix composite is described in this work which has advantageous thermo-elastic properties. These are shown to be advantageous in the integration of optical systems in Section IV. The composite consists of an aluminum matrix with embedded shape memory alloy (SMA) ribbons. The SMA ribbons served to restrict the thermal expansion of the parent aluminum matrix along the ribbon direction while the coefficient of thermal expansion (CTE) in directions normal to the ribbons remain close to the CTE of aluminum. This has particular utility for high performance optical metering structures, described in Section IV. Sections I-III detail the behavior and fabrication of the composite along with measurements of its thermo-elastic response.

Low expansion materials have been of interest for some time and include ceramics, metals, and composites. ZERODUR is a low expansion glass with near zero CTE that has found abundant use as optical elements in imaging systems designed to maintain performance in the presence of temperature changes [20.] Its application does not extend beyond optical elements since it has poor structural qualities (ductility and density.) A challenge then in the design of high performance optical systems is to provide a structural material which can match the CTE of ZERODUR and other low expansion glasses. Other low expansion materials that do serve as structural members include silicon carbide [23], aluminum-silicon [24],

Copyright © 2013 by ASME

Downloaded From: http://proceedings.asmedigitalcollection.asme.org/ on 05/14/2015 Terms of Use: http://asme.org/terms

aluminum-silicon carbide [28], and invar [22.] Silicon carbide has a high strength weight ratio but is brittle and involves a complex manufacturing process that can limit its form. Aluminum-silicon and aluminum-silicon carbide are promising materials with excellent structural qualities but have not achieved a CTE lower than 7 ppm/K. This is a significant improvement over aluminum (24 ppm/K) but can still introduce significant errors when paired with near zero CTE glasses. Invar is probably the most common structural material paired with low expansion glasses because of its low CTE (0.5 ppm/K) and good ductility and strength. Its key drawbacks are density and thermal conductivity. As such, invar structures tend to be heavy introduce optical errors from thermal gradients. Carbon/epoxy composites are also used; these can have a near zero CTE in tube form [26.] Other geometries do not in general have a low CTE and carbon/epoxy composites are challenging to integrate

Recent progress has been made in the area of composites for low thermal expansion. Negative expansion fillers have been developed but remain a challenge to combine with matrix materials [27.] An alternate approach is to use ordinary metals such as aluminum and titanium and combine them in a geometry that uses kinematics to achieve near zero CTE. Initial attempts yielded designs that are too difficult to manufacture [21] but a newly proposed kinematic design has been fabricated in a limited shape [19.] The composite proposed here uses the extraordinary response of SMAs which can have an effective CTE of -8% to balance the expansion of aluminum. The composite is enabled by the ultrasonic additive manufacturing process, unique in that metals are bonded under low temperature. The CTE can be tailored along the SMA ribbon direction by varying the volume fraction of SMA. Key contributions of this work are a modeling framework to predict CTE, a fabrication process for embedding super-elastic NiTi, and an experimental investigation of the dimensional stability and CTE of the resulting aluminum-NiTi composite.

I. BEHAVIOR AND MODELING

Development of a thermal invariant composite requires a model for the SMA and matrix. We combine the phenomenological SMA composite framework outlined by Sittner [4-7] with the addition of an underlying SMA formulation of a bivariant model developed by Brinson [8, 9]. The resulting model relies only on the properties of the composite's constituent materials. The model describes the behavior of a long-fiber reinforced SMA composite when subjected to a variable stress-temperature loading.

SMA New Bivariant Model

The foundation of the bivariant model for the SMA begins with the constitutive model by Brinson [8, 9] for one dimensional SMAs, which relates the macro-scale stress, strain, temperature and martensitic volume fraction through

$$\sigma - \sigma_o = E(\xi)\varepsilon - E(\xi_o)\varepsilon_o + \Omega(\xi_s)\xi_s - \Omega(\xi_o)\xi_{so} + \Theta(T - T_o), \quad (1)$$

where $E(\xi)$ is the elastic modulus, $\Omega(\xi)$ is the transformation tensor, and Θ is the stress-temperature coefficient. In the above equation,

$$\Omega = -E(\xi)\varepsilon_L \quad (2)$$

and

$$\Theta = E(\xi)\alpha. \quad (3)$$

Here, α is the coefficient of thermal expansion and ε_L is the maximum transformation strain. Important to the model is the separation of the martensitic volume fraction into two components, the stress-induced and temperature-induced volume fractions, ξ_S and ξ_T, respectively, as given in

$$\xi = \xi_S + \xi_T. \quad (4)$$

By considering the process:

$$\begin{aligned} d\sigma &= Ed\varepsilon + \Theta dT + \Omega d\xi_s \\ d\sigma &= Ed\varepsilon + \Theta dT + \Omega d\xi_s \\ d\sigma &= Ed\varepsilon - E\alpha dT - E\varepsilon_L d\xi_s \\ \tfrac{1}{E}d\sigma &= d\varepsilon - \alpha dT - \varepsilon_L d\xi_s \\ \Rightarrow d\varepsilon &= \frac{1}{E}d\sigma + \alpha dT + \varepsilon_L d\xi_s \end{aligned} \quad (5)$$

and applying current (σ, ε, T, ξ_T, ξ_s) and initial conditions (σ_o, ε_o, T_o, ξ_{To}, ξ_{so}) for stress, strain, temperature and volume fractions, the constitutive equation is rearranged to provide strain in terms of stress, temperature, and volume fraction:

$$(\varepsilon - \varepsilon_o) = \tfrac{1}{E}(\sigma - \sigma_o) + \alpha(T - T_o) + \varepsilon_L(\xi_s - \xi_{so}). \quad (6)$$

In this model, the volume fraction of martensitic NiTi is first calculated using the equations developed by Liang and Rogers [10, 11] from which the stress and temperature-induced volume fractions can then be calculated. Liang and Rogers give

$$\xi = \tfrac{1-\xi_o}{2}\cos\left[a_M\left(T - M_f^\sigma\right)\right] + \tfrac{1+\xi_o}{2} \quad (7)$$

for the reverse (A – M) transformation, where C_M is the martensitic stress-influence coefficient, M_f^σ is the stress-dependent martensitic start temperature, represented by

$$M_f^\sigma = M_f + \frac{\sigma}{C_M}, \quad (8)$$

and a_M is given by

$$a_M = \frac{\pi}{M_s - M_f}, \quad (9)$$

Copyright © 2013 by ASME

Downloaded From: http://proceedings.asmedigitalcollection.asme.org/ on 05/14/2015 Terms of Use: http://asme.org/terms

where M_s is the martensitic start temperature. Considering the forward direction, the equation for volume fraction becomes

$$\xi = \frac{\xi_o}{2}[\cos[a_A(T - A_s^\sigma)] + 1]. \quad (10)$$

Here, C_A is the austenite stress-influence coefficient, A_s^σ is the stress-dependent austenitic start temperature, given by

$$A_s^\sigma = A_s + \frac{\sigma}{C_A},$$

and a_A is given by

$$a_A = \frac{\pi}{A_f - A_s}. \quad (11)$$

With the value of the total martensitic volume fraction known, the stress and temperature-induced components are determined according to the new bivariant model. The phase diagram for the original bivariant model, which considers stress-independent martensite start and finish temperatures below the critical finish stress, varies from the new phase diagram, which is based on models that maintain stress-dependent martensitic transformation temperatures, which are presented in Figure 1 (a) and (b), respectively [9, 12, 13, 14, 15, 16].

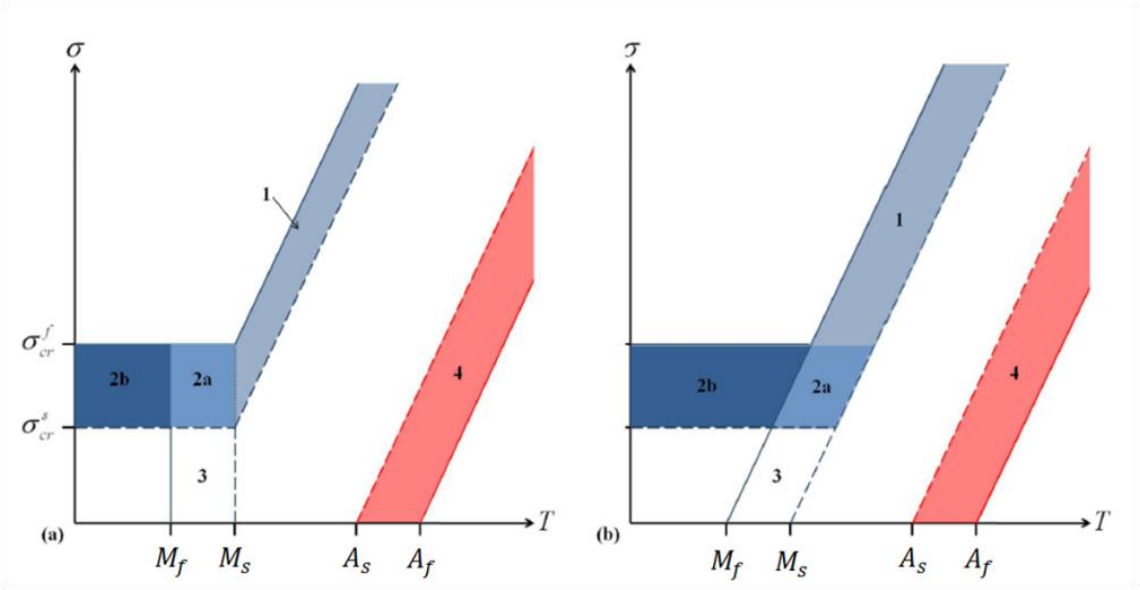

FIGURE 1 - STRESS-TEMPERATURE PHASE DIAGRAM IN (A) ORIGINAL BIVARIANT MODEL [8]; (B) NEW BIVARIANT MODEL.

Considering the M – A transformation, the stress and temperature-induced components depend only on the total volume fraction and the initial volume fractions prior to transformation. These components are given by [8]

$$\xi_T = \xi_{To} - \frac{\xi_{To}}{\xi_o}(\xi_o - \xi) \quad (12)$$

$$\xi_s = \xi_{so} - \frac{\xi_{so}}{\xi_o}(\xi_o - \xi). \quad (13)$$

Differing from the initial bivariant model are the regions 1, 2a, and 2b, which results in adaptations of the equations for the stress and temperature-induced components, which consider not only the transformation from austenite to martensite, but also the transformation from twinned to detwinned martensite. Considering region 1, which defines high-temperature stress-induced transformation, the new component equation becomes

$$\xi_s^{R1} = \frac{1-\xi_{so}}{2}\cos\left[a_M\left(T - M_f^\sigma\right)\right] + \frac{1+\xi_{so}}{2} \quad (14)$$

which is valid when $M_f^\sigma \le T \le M_s^\sigma$. For the low-temperature, stress-induced transformation region 2b, defined when $T < M_f^\sigma$ and $\sigma_{cr}^s \le \sigma \le \sigma_{cr}^f$, the components are given by

$$\xi_s^{R2b} = \frac{1-\xi_{so}}{2}\cos\left[\frac{\pi}{\sigma_{cr}^s - \sigma_{cr}^f}\left(\sigma - \sigma_{cr}^f\right)\right] + \frac{1+\xi_{so}}{2} \quad (15)$$

$$\xi_T^{R2b} = \xi_o - \xi_s^{R2b}. \quad (16)$$

Finally, region 2a is a region of mixed stress and temperature-induced transformation, which vary independently based upon the loading path. Within this region, there is a smooth transition between the transformation surfaces of region 1 and 2b. This is achieved via cosine functions which work to match the existing kinematic equations from the original bivariant model. To achieve this, the following form for the stress-induced martensite volume fraction is given as

$$\xi_s^{R2a} = \xi_T^{Mod} \times \xi_s^{Mod} + \xi_{so}, \quad (17)$$

where ξ_s^{Mod} is the stress modifier and ξ_T^{Mod} is the temperature modifier. The modifiers are given by

Copyright © 2013 by ASME

Downloaded From: http://proceedings.asmedigitalcollection.asme.org/ on 05/14/2015 Terms of Use: http://asme.org/terms

$$\xi_S^{Mod} = \left(\frac{1-\xi_{so}}{2}\right)\left[\cos\left[\frac{\pi}{\sigma_{cr}^s-\sigma_{cr}^f}\left(\sigma-\sigma_{cr}^f\right)\right]+1\right] \quad (18)$$

and

$$\xi_T^{Mod} = \left(\frac{1}{2}\right)\left[\cos\left[a_M\left(T-M_f^\sigma\right)\right]+1\right]. \quad (19)$$

Composite Model

With the new bivariant model established, the development of the composite model is achieved through the matching of strains between the matrix and the fibers. This matching process relies upon the material parameters of the component materials for the composite. In the end, the exact behavior and magnitude of the strain is dependent upon the modulus and CTE of the fiber and the matrix, as well as the amount of prestrain present within the SMA. The contribution of the SMA prestrain to the overall behavior of the composite is illustrated in Figure 2.

The strain matching approach assumes that the strain in the SMA fiber, ε_f, and strain in the matrix, ε_m, are equal. The fiber strain is described in (6) and the matrix strain is described as a typical thermoelastic response:

$$\varepsilon_m = \frac{1}{E_m}(\sigma_m - \sigma_{mo}) + \alpha_m(T - T_o) \quad (20)$$

where E_m is the elastic modulus of the matrix, σ_m is the stress in the matrix and α_m is the CTE of the matrix. Expanding the above equation and substituting in for the fiber strain

$$\frac{1}{E_f}\left(\sigma_f - \sigma_{fo}\right) + \alpha_f(T - T_o) + \varepsilon_L(\xi_s - \xi_{so})$$

$$= \frac{1}{E_m}(\sigma_m - \sigma_{mo}) + \alpha_m(T - T_o) \quad (21)$$

where E_f and σ_f are the fiber modulus and stress, respectively. Assuming no external loads and balancing forces, the stress in the matrix is determined by:

$$\sigma_f A_f + \sigma_m A_m = 0$$

$$\sigma_m = -\frac{A_f}{A_m}\sigma_f \quad (22)$$

$$\sigma_m = \frac{-v}{(1-v)}\sigma_f$$

where A_f and A_m are the cross-sectional areas of the fiber and matrix, respectively, and v is the fiber volume fraction. The variable change from the cross-sectional area to fiber volume fraction

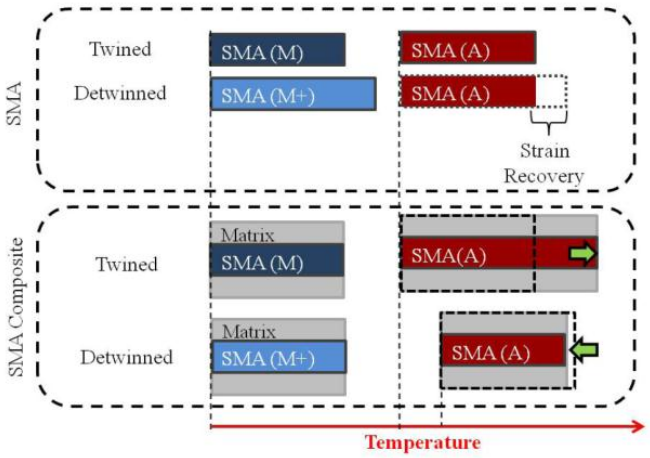

FIGURE 2 – THE EFFECT OF SMA PRESTRAIN ILLUSTRATED FOR IN UNCONSTRAINED SMA ELEMENT AND FOR A COMPOSITE WITH AN EMBEDDED SMA ELEMENT. IN THE UNCONSTRAINED STATE, THE SMA WILL RECOVER ANY STRAIN INDUCED DURING DETWINNING. WHEN CONSTRAINED BY THE COMPOSITE MATRIX, THE RECOVERY OF THE STRAIN OR GENERATION OF BLOCKING STRESS REDUCE THE AMOUNT OF THERMALLY-INDUCED COMPOSITE STRAIN.

can be made by assuming the fibers provide long-fiber reinforcement of the matrix and the lengths of the components are equal, $L_f = L_m = L$:

$$v = \frac{v_f}{v_{tot}}$$

$$v = \frac{v_f}{v_f+v_m} \quad (23)$$

$$v = \frac{A_f L}{A_f L + A_m L}$$

$$v = \frac{A_f}{A_f+A_L}.$$

Assuming zero initial stress, the stress in the SMA can be evaluated as a function of temperature, material properties, volume fraction, and transformation terms by substituting (22) into (21),

$$\frac{1}{E_f}\sigma_f + \alpha_f(T - T_o) + \varepsilon_L(\xi_s - \xi_{so})$$

$$= \frac{1}{E_m}\left(\frac{-v}{(1-v)}\sigma_f\right) + \alpha_f(T - T_o) \quad (24)$$

and solving for σ_f:

$$\sigma_f = \frac{(\alpha_m-\alpha_f)(\Delta T)}{\frac{1}{E_f}+\frac{1}{E_m}\frac{v}{(1-v)}} - \frac{\varepsilon_L(\xi_s-\xi_{so})}{\frac{1}{E_f}+\frac{1}{E_m}\frac{v}{(1-v)}}. \quad (25)$$

Copyright © 2013 by ASME

Downloaded From: http://proceedings.asmedigitalcollection.asme.org/ on 05/14/2015 Terms of Use: http://asme.org/terms

This equation has two components: the first is the thermoelastic component, which applies to any long-fiber reinforced composite; the second is due to the transformation-induced strain recovery of the SMA if it is embedded in a detwinned state. If the embedded SMA elements are not prestrained before fabrication, only the thermoelastic stress component remains but is non-linear due to the change in modulus during transformation. Once the SMA stress is calculated, it is used to determine the total composite strain:

$$\varepsilon_{comp} = \varepsilon_f = \frac{1}{E_f}\left[\frac{(\alpha_m - \alpha_f)(\Delta T)}{\frac{1}{E_f}+\frac{1}{E_m}\frac{v}{(1-v)}} - \frac{\varepsilon_L(\xi_s - \xi_{so})}{\frac{1}{E_f}+\frac{1}{E_m}\frac{v}{(1-v)}}\right] + \alpha_f(\Delta T) + \varepsilon_L(\xi_s - \xi_{so}). \quad (26)$$

Expanding (23) gives

$$\varepsilon_{comp} = \frac{E_f v\alpha_f + E_m(1-v)\alpha_m}{E_f v + E_m(1-v)}\Delta T - \frac{E_f v\varepsilon_L(\xi_{so}-\xi_s)}{E_f v + E_m(1-v)}. \quad (27)$$

The same result is obtained by calculating the matrix stress and using it in (20). If the stress-induced martensitic volume fraction term is ignored, the first component of the strain equation in (27) describes the thermally-induced strain for a typical long-fiber reinforced composite [17, 18]. The second term is unique to SMA composites.

II. FABRICATION

Utilizing the models developed for the performance of a metal matrix composite (MMC) with embedded SMA fibers, a coupon was designed with Al-3003 being the matrix material and pseudoelastic NiTi the material of the fibers. The proposed design was one having 17.2% volume fraction of pseudoelastic NiTi and a point of zero CTE at 58°C, Figure 3[2].

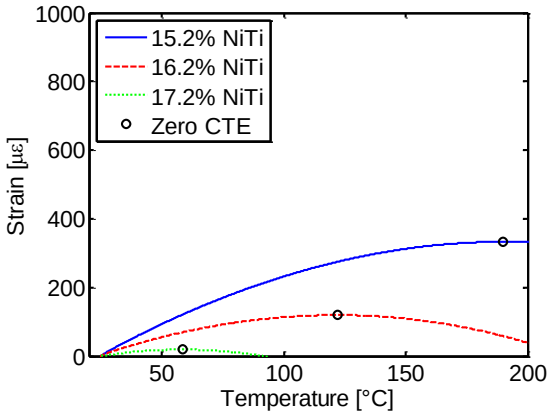

FIGURE 3 - STRAIN VERSUS TEMPERATURE FOR AL-3003/PSEUDOELASTIC-NITI COMPOSITE WITH VARYING VOLUME FRACTIONS OF NITI. ZERO-CTE POINTS ARE IDENTIFIED FOR EACH VOLUME FRACTION WITH BLACK CIRCLES.

To obtain the necessary volume fraction of NiTi, different cross-sectional designs were engineered, with the final design having eight pseudoelastic NiTi ribbons embedded within the matrix, Figure 4. As shown, the ribbons were embedded between layers of aluminum through Ultrasonic Additive Manufacturing (UAM). In order to achieve zero-CTE as described by the model, the pseudoelastic NiTi needed to be strained by 8% in order to fully obtain detwinned martensite (M^+).

The process used to achieve the metal matrix composite with embedded SMA involved multiple steps including straining the pseudoelastic material, transferring the ribbons between various clamps, and performing the welding. The method for obtaining detwinned martensite consists of straining the NiTi by applying a tensile load with free weights. Based on characterization studies of the specific NiTi to be embedded, the required load was 3.86 kg (8.50 lb) per ribbon. The layers consisting of three and two ribbons were loaded by 11.57 kg (25.50 lb) and 7.71 kg (17.00 lb) respectively. Once the ribbons were strained to M^+, they were secured in a fixture that was designed to transfer the ribbons from the detwinning clamps to the base plate. The base plate is the foundation for the UAM process, where the sacrificial build plate and ribbons are fixed while the ultrasonic metal welding occurs.

Copyright © 2013 by ASME

Downloaded From: http://proceedings.asmedigitalcollection.asme.org/ on 05/14/2015 Terms of Use: http://asme.org/terms

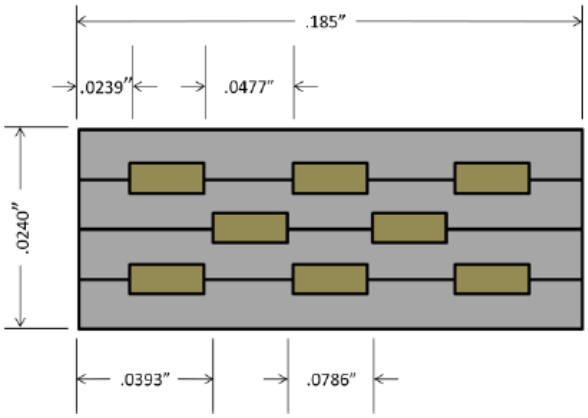

FIGURE 4 - PROPOSED GEOMETRY FOR AL-3003/PSEUDOELASTIC NITI COMPOSITE TO ACHIEVE 17.2% VOLUME FRACTION NITI.

The production of the first coupon, Composite P-1, with the desired 17.2% volume fraction was performed using a single clamp to fix the detwinned ribbons to the base plate. This process worked well for the first and second ribbon layer, with minor recovery of the pre-strain in the ribbons. The third ribbon layer did not produce an accurate cross-section, as the ribbons recovered a majority of the prestrain and drifted from the desired locations, Figure 5. Cross-sectional measurements following the build process identified Composite P-1 as having a volume fraction of 9.78% pseudoelastic NiTi.

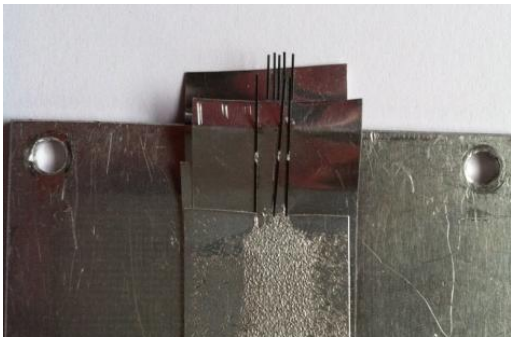

FIGURE 5 - TOP VIEW OF COMPOSITE P-1 WITH SEPARATION OF RIBBONS FROM PROPOSED GEOMETRY.

Analysis of the production method suggests that the recovery of the prestrain within the NiTi ribbons was the result of ultrasonic lubrication, or the process by which a reduction in friction is achieved via vibrations in excess of 20 kHz [1]. In this application, the vibrations from the welding horn traveled through the ribbons to the clamp, where the ribbons were able to slip. Modifications were made to the method by which the ribbons were secured to the base plate for the purpose of damping the vibrations from the welder. The result was an additional series of clamps for the ribbons, which would assist in dissipating the vibrations which were transferred by the ribbons. The final process for fabrication of the composite design was obtained with this design, Figure 5.

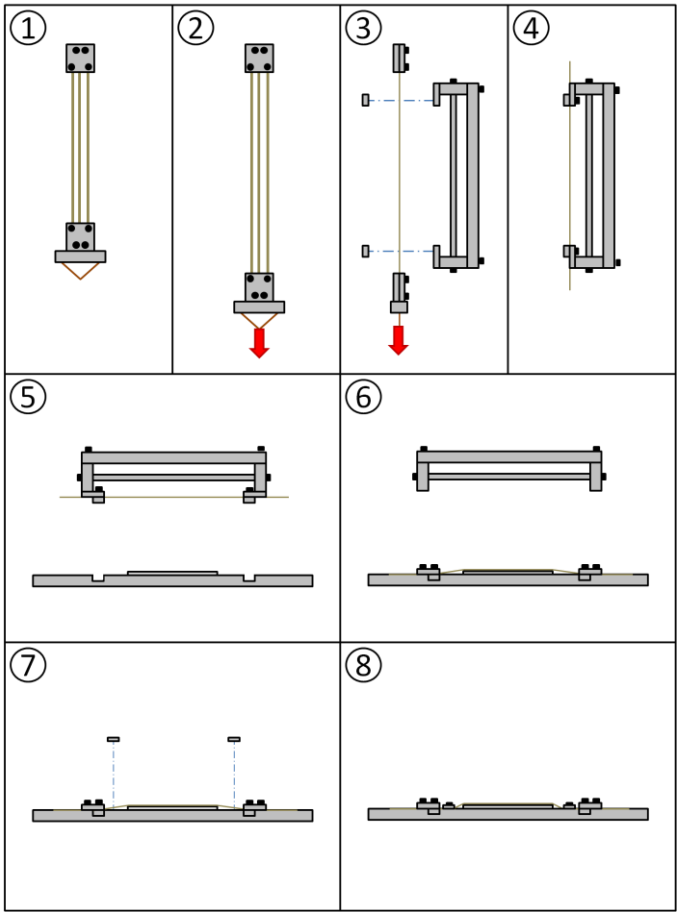

FIGURE 5 – FABRICATION PROCESS FOR PRODUCING AL-3003 / PSEUDOELASTIC NITI COMPOSITE WITH VOLUME FRACTION OF 17.2% NITI. (1) THE NITI RIBBONS ARE LOADED INTO THE DETWINNING CLAMPS. (2) THE UPPER DETWINNING CLAMP IS HELD FIXED WHILE A FORCE STRETCHES THE RIBBONS. THE FORCE IS PREDETERMINED BASED ON THE REQUIRED STRAIN. (3) WHILE THE RIBBONS ARE KEPT IN A STRAINED STATE, A TRANSFER CLAMP IS USED TO SECURE THE RIBBONS. (4) WITH THE STRAINED RIBBONS HELD IN THE TRANSFER CLAMP, THE DETWINNING CLAMPS ARE REMOVED FROM THE RIBBONS. (5) THE TRANSFER CLAMP IS LINED UP WITH SLOTS ON THE BASE PLATE. (6) ONCE THE RIBBONS ARE IN THE CORRECT POSITION, THE BOTTOMS OF THE LEFT AND RIGHT UPRIGHTS ARE BOLTED TO THE BASE PLATE, AFTER WHICH THE REMAINING PORTIONS OF THE TRANSFER CLAMP ARE REMOVED, LEAVING THE RIBBONS IN THEIR STRAINED STATE. (7) ANOTHER SET OF RIBBON CLAMPS ARE LINED UP. (8) THE SECOND SET OF RIBBON CLAMPS ARE BOLTED TO THE BASE PLATE, SECURING THE RIBBONS TWICE ON EACH SIDE OF THE BUILD PLATE, WHICH IS MOUNTED TO THE MIDDLE OF THE BASE PLATE.

Copyright © 2013 by ASME

Downloaded From: http://proceedings.asmedigitalcollection.asme.org/ on 05/14/2015 Terms of Use: http://asme.org/terms

Following the new process, a new composite, Composite P-2, was constructed with the same 17.2% NiTi geometry. The resulting design was more accurate in cross-section than Composite P-1, Figure 6.

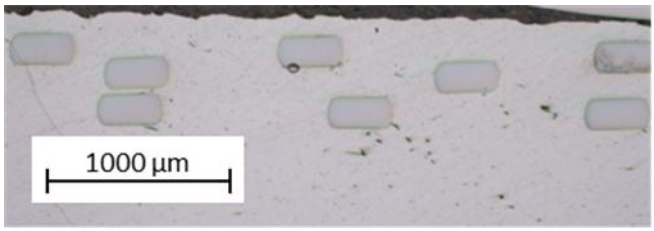

FIGURE 6 - MICROGRAPH OF CROSS-SECTION OF COMPOSITE P-2.

The volume fraction of Composite P-2 is 16.1% pseudoelastic NiTi, a percentage less than the target volume fraction.

III. EXPERIMENTAL

Initial studies of Composites P-1 and P-2 were performed for the determination of the coefficient of thermal expansion with a focus on identifying a point where this value is zero. To do this, thermal cycles were performed on separate occasions in a thermal chamber which housed the composite as well as a reference sample of 3000 series aluminum. The temperature of the chamber was increased from room temperature (RT) to 100°C before being cooled back to RT. Throughout this time, strain gauges on the top and bottom of the samples were used to measure the strain of both samples within the chamber. The measured strains from the top and the bottom gauges were averaged to determine the strain of each individual sample. The purpose of having the reference aluminum sample is to use the strain read-outs from this sample to remove the thermal dependency of the strain gauges from the composite's strain [2]. This was calculated by subtracting the reference sample's strain from the composite's and then adding in the known value of the aluminum strain based on temperature change, which in total is given by [2],

$$\varepsilon_{comp} = \varepsilon_{sig/comp} - \varepsilon_{sig/ref} + \alpha_{ref}\Delta T. \quad (28)$$

Here, $\varepsilon_{sig/comp}$ is the non-compensated strain from the composite, $\varepsilon_{sig/ref}$ is the strain from the reference sample, α_{ref} is the CTE of the reference aluminum (23.2 με/°C [3]), and ΔT is the change in temperature.

The thermal cycles for the determination of the coefficient of thermal expansion were first performed on Composite P-1. Three thermal cycles were performed from which the CTE values, Table 1, were determined for each cycle on both the increasing and decreasing temperature portions of the cycle by using the *polyfit* command in MATLAB.

TABLE 1 - CTE VALUES FOR COMPOSITE P-1 AS DETERMINED BY THERMAL CYCLING FROM RT TO 100°C AND BACK TO RT.

Temperature Region of Cycle	Coefficient of Thermal Expansion, [με/°C]		
	Cycle 1	Cycle 2	Cycle 3
Increasing	20.70	20.80	20.84
Decreasing	20.77	21.28	20.85

For Composite P-1, the CTE averaged 20.94 με/°C, which is only 9.7 % different from the CTE of aluminum and over four times higher than the target value of 5 με/°C. The high values of CTE for Composite P-1 confirm the inaccurate volume fraction and the recovery of the prestrain of the NiTi in Composite P-1.

Thermal cycling was repeated for Composite P-2 with the number of cycles being six, Figure 7. The resulting CTE values for Composite P-2 through the first six thermal cycles, Table 2, are closer to the desired values, with an average of 13.83 με/°C, a 40.4% decrease in CTE relative to aluminum.

Copyright © 2013 by ASME

Downloaded From: http://proceedings.asmedigitalcollection.asme.org/ on 05/14/2015 Terms of Use: http://asme.org/terms

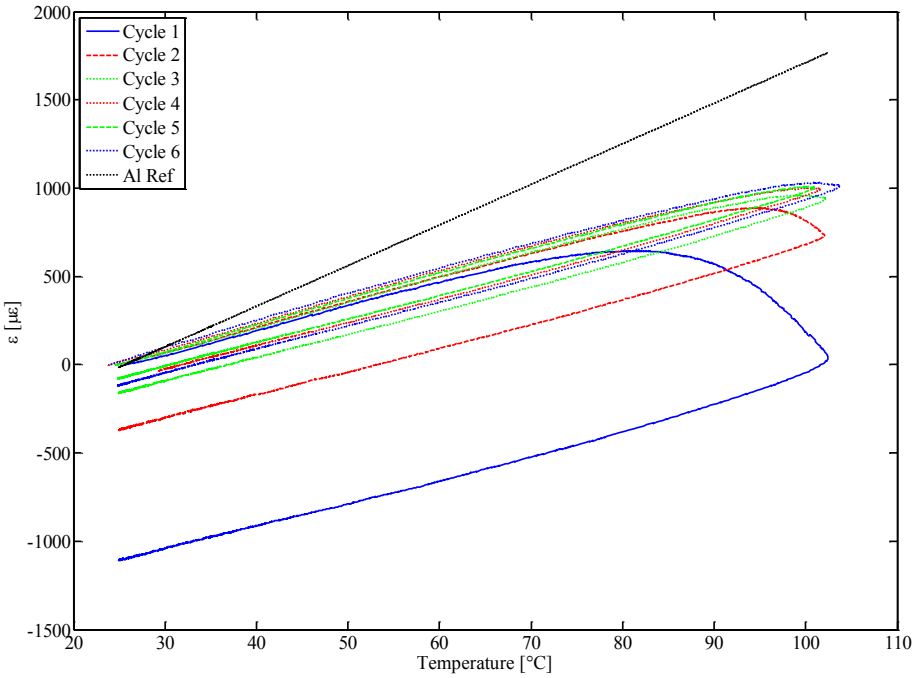

FIGURE 7 - STRAIN VERSUS TEMPERATURE FOR SIX INITIAL THERMAL CYCLES OF COMPOSITE P-2.

TABLE 2 - CTE VALUES FOR COMPOSITE P-1 AS DETERMINE BY THERMAL CYCLING FROM RT TO 100°C AND BACK TO RT.

Temperature Region of Cycle	Coefficient of Thermal Expansion, [με/°C]					
	Cycle 1	Cycle 2	Cycle 3	Cycle 4	Cycle 5	Cycle 6
Increasing	13.86	13.72	14.07	14.34	14.41	14.17
Decreasing	13.43	13.51	13.57	13.58	13.62	13.64

Composite P-2 exhibits irrecoverable strains, i.e., the strain of the composite does not return to the initial strain value of each cycle, as graphically shown in Figure 7 by the gap between the start and end points of each cycle. Tests were performed to study the effects of extended periods of time at elevated temperature. These extended elevated temperature tests looked at temperatures starting around 50°C and progressed in increments of approximately 10°C until reaching around 100°C, Figure 8. The test started with the composite at RT and heated it to the set incremental temperature value, where it was then held for 30 minutes. Following the duration of held temperature, the composite was then cooled back to RT.

Copyright © 2013 by ASME

Downloaded From: http://proceedings.asmedigitalcollection.asme.org/ on 05/14/2015 Terms of Use: http://asme.org/terms

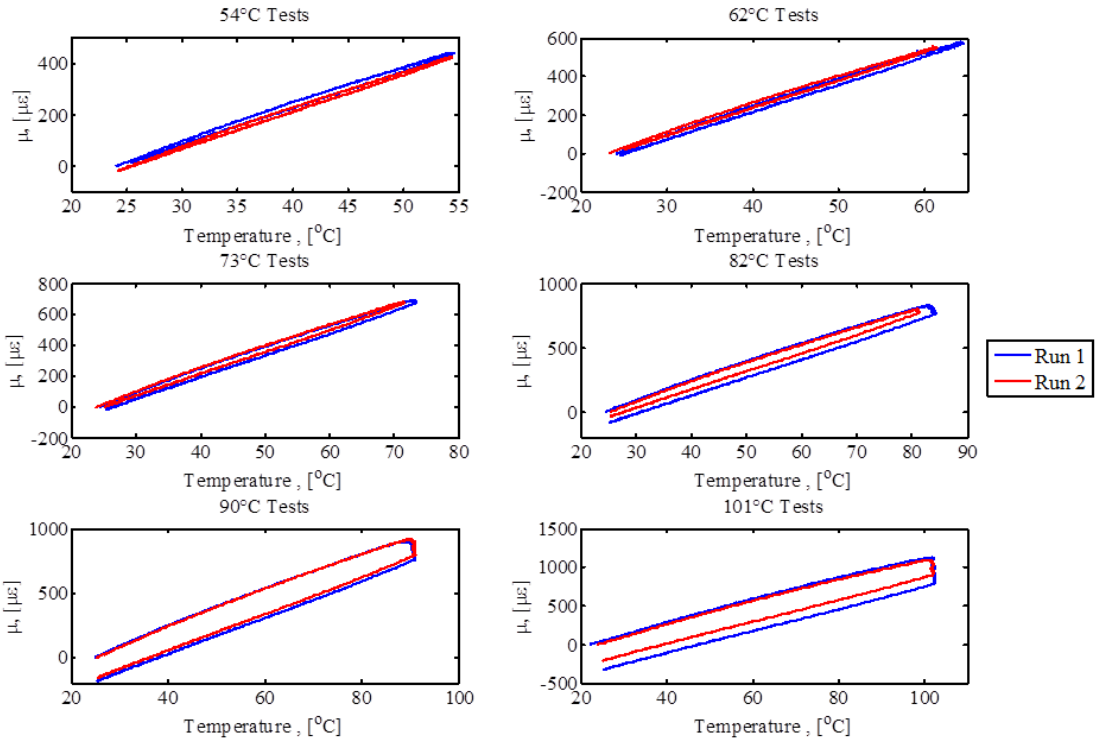

FIGURE 8 - RESULTS OF EXTENDED ELEVATED TEMPERATURE TESTS ON COMPOSITE P-2.

A correlation between the temperature to which the composite is heated and the irrecoverable strain is displayed by the results of the extended elevated temperature tests, as there is less than 10 με that is irrecoverable during the 54°C and 62°C tests and over 200 με that is irrecoverable for the 101°C test.

Subsequent tests were completed to consider the influence of time on the irrecoverable strain within Composite P-2. A series of tests were performed by heating the samples to approximately 100°C, as this temperature would provide better resolution since the greatest amount of irrecoverable strain occurred at the highest temperatures during the extended elevated temperature tests. Variations in the duration at which the composite was held at 101°C were 0.5, 1, 2, 3.5, and 4 hours, Figure 9. The points for heating and cooling were based on the composite's temperature, therefore, the time values may vary from one test to another as thermal parameters caused slight variations between the tests. Time's effect on the irrecoverable strain was not proportional, where the amount of irrecoverable strain did not increase with the amount of time the composite was held at 101°C. Instead, the strain rate from one cycle to the next decreased in a non-linear fashion, Figure 10, which is given by the successively shallower slopes in Figure 9.

Copyright © 2013 by ASME

Downloaded From: http://proceedings.asmedigitalcollection.asme.org/ on 05/14/2015 Terms of Use: http://asme.org/terms

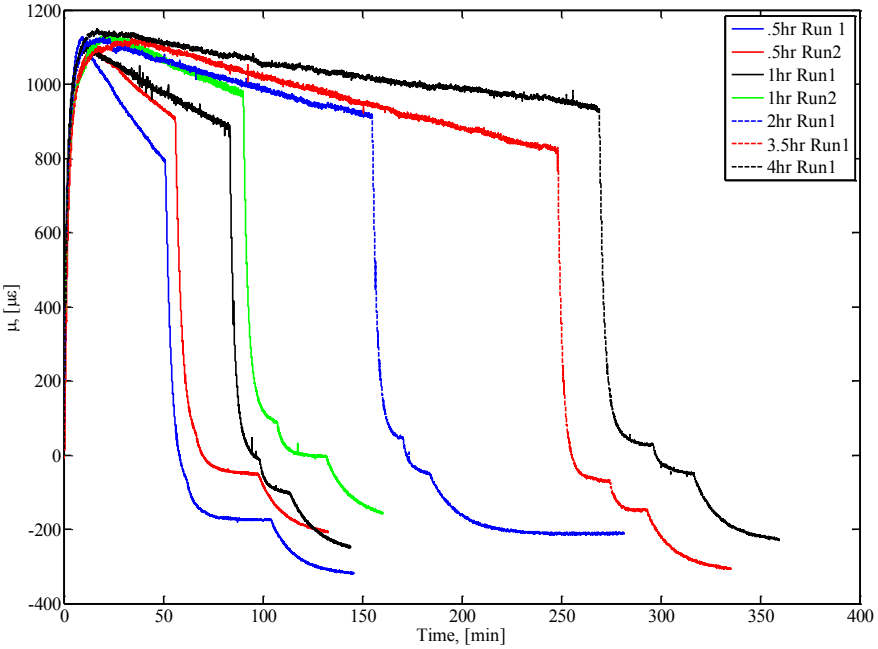

FIGURE 9 - STRAIN VERSUS TIME FOR 101°C TESTS PERFORMED ON COMPOSITE P-2, WHERE THE ORDER OF THE RUNS IS GIVEN BY THE ORDER OF THE LEGEND FROM TOP TO BOTTOM.

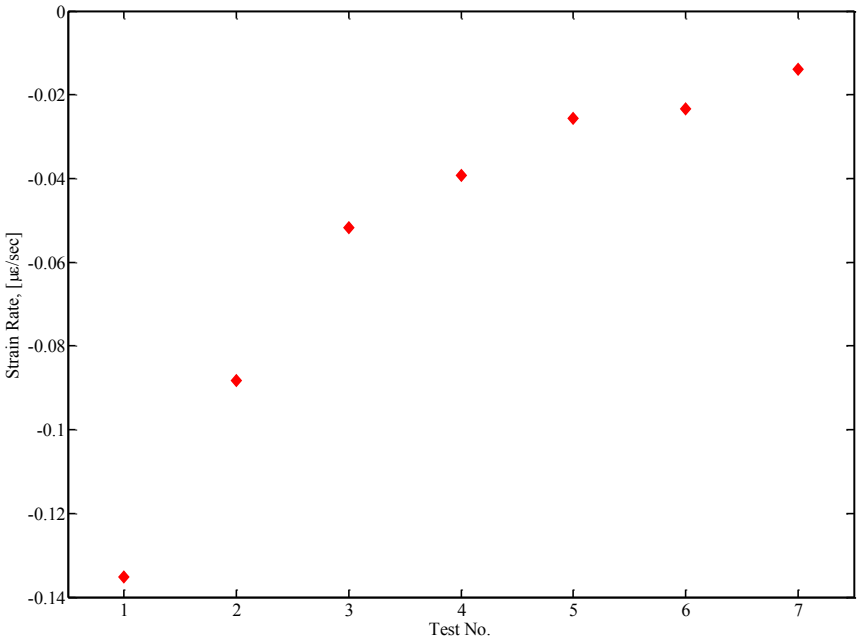

FIGURE 10 - STRAIN RATES FOR EFFECTS OF TIME ON IRRECOVERABLE STRAIN TESTS AT 101°C.

Copyright © 2013 by ASME

Downloaded From: http://proceedings.asmedigitalcollection.asme.org/ on 05/14/2015 Terms of Use: http://asme.org/terms

IV. DISCUSSION AND SYSTEM INTEGRATION

It's been shown that introduction of NiTi ribbons into an aluminum matrix results in a CTE that is significantly lower than aluminum (~40%.) While measurements weren't shown here, it's expected that the CTE normal to the ribbons remains near the 24 ppm/K of aluminum. This anisotropic behavior has significant advantages in the integration of optical systems. Figure 11 illustrates the need for an optical support structure to match the CTE of a mirror in the direction of light. The cartoon depiction shows the deformation of a simple assembly of a mirror mounted on a beam at temperature 2 higher than temperature 1. From temperature 1 to temperature 2, the radius of curvature of the mirror changes as the product of its CTE and radius of curvature. The length of the beam at temperature 1 is chosen as the radius of curvature so that its change in length from temperature 1 to temperature 2 is the product of its CTE and the radius of curvature of the mirror. If the CTE of the beam matches the mirror then the focal point is unchanged and the design is athermal. This simple design assumes isothermal conditions, thus a high thermal diffusivity material is desirable to avoid temperature gradients.

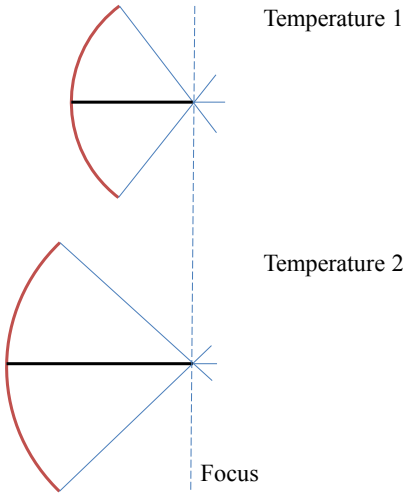

FIGURE 11 - CARTOON DEPICTION OF A SPHERICAL LENS AND MOUNTED ON A BEAM AT TWO TEMPERATURES

Optical subassemblies are typically mounted to an aluminum optical bench, especially in space and airborne applications where weight is constrained. This presents a challenge for mechanical integration when there is a CTE mismatch between the optical support structure (the beam in Figure 11) and the optical bench. This mismatch can cause a buildup of loads across the bolt pattern resulting in deformation of the support structure and optical path errors.

An advantage then of the aluminum-NiTi composite presented here is that there is very little CTE mismatch in directions normal to the NiTi ribbons. This offers a similar advantage for the mirror mount where the mirror can be bonded in an aluminum bezel which is easily integrated to an aluminum-NiTi support structure. When invar support structures are used, the bezel is necessarily invar to match the CTE. Replacing invar support structures and lens bezels with an aluminum-NiTi composite could potentially reduce the weight by 2/3rds. Optical errors from temperature gradients would also be reduced owing to the high thermal diffusivity of aluminum relative to invar.

While the theory shown in Section I promises the possibility of a near 100% reduction in the CTE of aluminum with addition of 17% NiTi by volume, measurements have shown a 40% reduction. Additionally, there is a large and unexpected irrecoverable strain developed. Future work will include a detailed study of the interface between the SMA ribbons and the aluminum to further investigate these discrepancies. Additional experiments will also be made with different volume fractions of NiTi.

REFERENCES

[1] Dong, S., & Dapino, M. J. (2012, March). Piezoelectrically-induced ultrasonic lubrication by way of Poisson effect. In *Proceedings of SPIE* (Vol. 8343, p. 83430L).

[2] Hahnlen, R. M. (2012). *Characterization and modeling of active metal-matrix composites with embedded shape memory alloys*.

[3] Kaufman, J. (1999). *Properties of Aluminum Alloys: Tensile, Creep, and Fatigue Data at High and Low Temperatures*. The Aluminum Association, Inc. and ASM International, Materials Park, OH.

[4] P. Sittner, V. Michaud, and J. Schrooten. Modeling and material design of SMA polymer composites. *Materials Transactions*, 43(5):984-993, 2002.

[5] P. Sittner and R. Stalmans. Developing hybrid polymer composites with embedded shape-memory alloy wires. *JOM*, 52(10):15-20, 2000.

[6] P. Sittner, R. Stalmans, and M. Tokuda. An algorithm for prediction of the hysteretic responses of shape memory alloys. *Smart Materials and Structures*, 9(4):452-465, 2000.

[7] P. Sittner, D. Vokoun, G. N. Dayananda, and R. Stalmans. Recovery stress generation in shape memory $Ti_{50}Ni_{45}Cu_5$ thin wires. *Materials Science and Engineering A*, 286:298-311, 2000.

[8] L. Brinson. One dimensional constitutive behavior of shape memory alloys. *Journal of Intelligent Material Systems and Structures*, 4(2):229-242, 1993.

[9] L. C. Brinson and M. S. Huang. Simpli_cation and comparisons of shape memory alloy constitutive models. *Journal of Intelligent Material Systems and Structures*, 7:108-114, 1996.

Copyright © 2013 by ASME

Downloaded From: http://proceedings.asmedigitalcollection.asme.org/ on 05/14/2015 Terms of Use: http://asme.org/terms

[10] C. Liang and C. A. Rogers. One-dimensional thermomechanical constitutive relations for shape memory materials. *Journal of Intelligent Material Systems and Structures*, 1:207-234, 1990.

[11] C. Liang and C. A. Rogers. One-dimensional thermomechanical constitutive relations for shape memory materials. *Journal of Intelligent Material Systems and Structures*, 8:285-302, 1997.

[12] C. Cismasiu and F. P. Amarante dos Santos. *Shape Memory Alloys*, chapter 7: Numerical simulation of a semi-active vibration control device based on superelastic shape memory alloy wires, pages 127-154. Sciyo, Rijeka, Croatia, 2010.

[13] D. J. Hartl and D. C. Lagoudas. *Shape Memory Alloys*, chapter 2: Thermomechanical Characterization of ShapeMemory Alloy Materials. Science and Business Media, LLC, New York, NY, 2008.

[14] Y. Ivshin and T. J. Pence. A constitutive model for hysteretic phase transition behavior. *International Journal of Engineering Science*, 32(4):681-704, 1994.

[15] Y. Ivshin and T. J. Pence. A thermomechanical model for a one variant shape memory material. *Journal of Intelligent Material Systems and Structures*, 5:455-7473, 1994.

[16] J. Zurbitu, S. Kustov, A. Zabalet, E. Cesari, and J. Aurrekoetxea. *Shape Memory Alloys*, chapter 2: Themo-mechanical behaviour of NiTi at impact, pages 17-39. Sciyo, Rijeka, Croatia, 2010.

[17] R. A. Schapery. Thermal expansion coe_cients of composite materials based on energy principles. *Journal of Composite Materials*, 2(3):380-404, 1968.

[18] G. Staab. *Laminar Composites*. Butterworth-Heinemann, Boston, MA, 1999.

[19] C. Steeves, S. dos Santos e Lucato, M. He, E. Antinucci, J. Hutchinson, and A. Evans. Concepts for structurally robust materials that combine low thermal expansion with high stiffness. *Journal of the Mechanics of Physics and Solids*, 55:1803-1822, 2007.

[20] Schott Optics. Thermal expansion of ZERODUR data sheet. *TIE-37*, Schott Optics, Duryea, PA, 2006.

[21] O. Sigmund and S. Torquato. Design of materials with extreme thermal expansion using a three-phase topology optimization method. *Journal of Mechanics of Physics and Solids*, 45:1037-1067, 1997.

[22] Rolled Alloys. Invar 36 Data Sheet. *Bulletin No. 1336USe*. Rolled Alloys, Temperance, MI, 2011.

[23] Ceradyne, inc. Silicon Carbide Data Sheet. *PDS #002 REV. NC*. Ceradyne, inc., Cost Mesa, CA, 2011.

[24] Materion Corporation. AMC225XE particle reinforced aluminum alloy. *MAMC 10.12*. Materion Corporation, Elmore, OH, 2011.

[25] R. Bohlman. Composite-to-metal joining. *ASM Handbook Volume 6, Welding, Brazing, and Soldering*. ASM International, 1993.

[26] Goodfellow. Carbon / epoxy composite materials – properties – supplier data by Goodfellow. Goodfellow, Cheshire, UK, 2011.

[27] C. Lind. Two decades of negative thermal expansion research: where do we stand? *Materials*, 5:1125-1154, 2012.

[28] Osprey. Osprey CE metals for thermal management. *Osprey publication 1817*, Sandvik Osprey, West Midlands, UK.

Copyright © 2013 by ASME

Downloaded From: http://proceedings.asmedigitalcollection.asme.org/ on 05/14/2015 Terms of Use: http://asme.org/terms